Varying chromaticity: A damping mechanism for the transverse head-tail instability

Wen-Hao Cheng,[1] Andrew M. Sessler,[2] and Jonathan S. Wurtele[1,2]
[1]*Department of Physics, University of California at Berkeley, Berkeley, California 94720*
[2]*Lawrence Berkeley National Laboratory, Berkeley, California 94720*
(Received 11 December 1996; revised manuscript received 27 May 1997)

A detailed analytical and numerical study of the suppression of the transverse head-tail instability by modulating the chromaticity over a synchrotron period is presented. We find that a threshold can be developed, and it can be increased to a value larger than the strong head-tail instability threshold. The stability criterion derived agrees very well with the simulations. The underlying physical mechanisms of the damping scheme are rotation of the head-tail phase such that the instability does not occur, and Landau damping due to the incoherent betatron tune spread generated by the varying chromaticity. [S1063-651X(97)02410-0]

PACS number(s): 29.27.Bd, 41.75.−i

I. INTRODUCTION

In particle accelerators, the interactions of the beam particles with its surroundings creates an electromagnetic field, the so-called wake field, which reacts and perturbs the beam, and can often lead to collective instabilities. These instabilities limit the beam current in accelerators. Many schemes have been devised to control these instabilities, such as the use of a BNS damping [1] for linear accelerators, and feedback systems for circular machines. In this paper, we describe a method for controlling such instabilities: through a temporal variation of the ring parameters. We exemplify this method by the suppression of the transverse head-tail (HT) instability by means of variation of the chromaticity [2].

When traveling in a storage ring, particles of different momentum can receive different transverse focusing strength, and thus have different betatron frequencies. Chromaticity ξ, defined as the ratio of the relative frequency difference to the relative momentum difference, gives the betatron angular frequency of an off-momentum particle as

$$\omega_\beta(\delta)=\omega_{\beta 0}(1+\xi\delta), \tag{1}$$

where $\omega_{\beta 0}$ is the betatron angular frequency of the on-momentum particle, and $\delta=\Delta p/p$ is the relative momentum difference. The longitudinal motion of a bunched beam is maintained by rf fields, and the particle's momentum oscillates with the synchrotron period.

When $\xi=0$, there is an instability in the particle's transverse motion called the strong head-tail (SHT) instability. This instability has a threshold which depends on bunch current, wake force, and synchrotron period. When the threshold is exceeded, the bunch's transverse motion blows up. When $\xi\neq 0$, there are both the SHT instability with a threshold and the HT instability. The HT instability, driven by the chromaticity, has no stability threshold. It was observed in experiments [3], has been well analyzed [4], and has been confirmed by simulations [5]. The HT instability is still a concern for many circular accelerators, for example (citing from the recent literature on the subject): the observations and simulations of single-bunch transverse excitation of the beam in the proton ring of the HERA (Hadron Electron Ring Anlage) collider at DESY (German Electron Synchrotron) [6], the observation of higher-order HT instability in the PS Booster of the Large Hadron Collider at CERN (European Organization for Nuclear Research) [7], and the investigation of the possible HT oscillation due to a transverse feedback kicker at the High Energy Accelerator Research Organization's B-Factory (KEKB) [8].

It can be seen that, from Eq. (1), the betatron frequency is varied by the momentum oscillation if there is chromaticity, and an integer resonance can be reached if ξ is too large. For most accelerators, ξ must be sufficiently minimized to avoid single-particle orbital resonances. Under this circumstance, analysis (by a moment expansion of the linearized Vlasov equation describing the coupled longitudinal and dipole transverse motions) [9] shows that the lowest-order mode has a large growth rate for $\xi/\eta<0$, and is strongly damped when $\xi/\eta>0$. Higher-order modes grow, with substantially smaller growth rates than the lowest-order mode, when $\xi/\eta>0$. They are damped for $\xi/\eta<0$. The growth rate of the instability depends on the magnitude of ξ/η and how the beam spectrum overlaps with the impedance (Fourier transform of the wake field) spectrum. Here $\eta=pdC/Cdp-1/\gamma^2$ is the slippage factor, $C=2\pi R=cT_0$ is the circumference of the ring, $\gamma=(1-\beta^2)^{-1/2}$, and we take $\beta=v/c\approx 1$.

As the sign of ξ/η is crucial to the stability of the lowest-order mode and higher-order modes of the head-tail oscillations, we consider, in analogy to the strong focusing effect (on collective modes, instead of on single particle orbits), alternating the sign of ξ within a synchrotron period to stabilize all modes. Two effects can be anticipated: first, an enhanced Landau damping from the incoherent tune spread induced by the chromaticity variation, and second, an otherwise accumulating chromatic effect during the synchrotron oscillation is canceled out if the sign of the chromaticity is reversed within a synchrotron period. Instead of varying η, we choose to vary ξ, since varying η means transition crossing, and therefore involves many undesirable phenomenon, such as vanishing Landau damping, large momentum spread, bunch-shape mismatch and nonlinear effects [10].

We were advised of the existence of the paper written by T. Nakamura [11], recently. Nakamura suggested, as we have also (independently), the concept of the varying chromaticity. In this paper, going considerably beyond what Na-

kamura has done, we provide a complete analysis, simulation results, and a stability criterion for the head-tail instability.

We assume the chromaticity is varied as

$$\xi(s)=\xi_0+\xi_1 \sin \phi_z(s), \tag{2}$$

which is no longer a constant but a function of ''time'' s, where s measures the distance around the ring, $\phi_z(s)=\omega_s s/c$ is the synchrotron phase advance, ω_s is the synchrotron angular frequency. The constant (dc) part of the chromaticity, ξ_0, causes the HT instability. The dc incoherent tune spread is not effective in stabilizing the HT instability. As will be shown, the ac part of the chromaticity, ξ_1, is introduced to provide an incoherent tune spread that suppresses the HT instability without causing additional instabilities.

In this work, we concentrate on the case of modulation of the chromaticity by the same period of the synchrotron oscillation. A faster modulation is of course also possible. In general, the chromaticity can be expanded in a Fourier series in terms of ϕ_z, as

$$\xi(s)=\xi_0+\sum_{n=0} \xi_n \cos(n\phi_z+\theta_n), \tag{3}$$

In Appendix A, we show that the periodicity of the varying chromaticity, n, must be an odd number, such that the ξ_n does not cause instability.

The lattice design may give a constant chromaticity with a significant nonlinear component ξ_{01}, in which $\xi_{DC}=\xi_0+\xi_{01}\delta$. This nonlinear component also generates an incoherent tune spread, but note that this tune spread is smaller by a factor σ_δ than the tune spread from the varying chromaticity, and is not significant in most cases. Here $\sigma_\delta=(\omega_s/c\,\eta)\sigma_z$ is the rms bunch energy spread, and σ_z is the rms bunch length.

In Sec. II, a Vlasov analysis is presented. We examine the growth rates for beams with a hollow distribution and with a Gaussian distribution, where both the contributions of the ac and dc parts are included. Results of macroparticle simulation are discussed.

In Sec. III, the effect of Landau damping, which is not considered in Sec. II, is included by the method of singular eigenfunction expansion. We provide an estimate for the damping rate, an approximate stability criterion, and a dispersion relation which includes the incoherent tune spread. We compare the stability limit with macroparticle simulations. The conclusion is given in Sec. IV.

II. VLASOV ANALYSIS

In this section, we derive a linear eigenmode equation which includes both the dc and ac parts of the chromaticity. As a starting point of the analysis, we calculate the coherent tune shift of a hollow beam and a Gaussian beam in the longitudinal phase space for arbitrary ξ_0 and ξ_1, neglecting any damping from the incoherent tune spread. The effect of the incoherent tune spread will be included in Sec. III.

We assume the particle in a bunched beam experiences two forces: the external focusing force and the wake force generated from the interaction between the beam and its environment. The transverse (for either vertical or horizontal) equation of motion for a particle in a bunch is

$$y''(z,s)+\frac{\omega_\beta^2(\delta)}{c^2}y(z,s) = -\frac{r_0}{\gamma C}\int_z^\infty dz'\rho(z')W_\perp(z-z')y(z',s), \tag{4}$$

where $y(z)$ is the transverse (longitudinal) oscillation amplitude with respect to the bunch center, the prime denotes d/ds, $N=\int dz'\rho(z')$ is the number of particles in a bunch, $r_0=e^2/m_0c^2$, $W_\perp$ is the transverse wake function, and the particle's energy is $E=\gamma m_0c^2$. The longitudinal motion is prescribed by

$$z=r_z \cos \phi_z, \quad \delta=(\omega_s/c\,\eta)r_z \sin \phi_z, \tag{5}$$

where (r_z,ϕ_z) are the action-angle variables in the longitudinal phase space, and we have neglected longitudinal wake force, nonlinear slippage factor, and synchrobetatron coupling.

There are three parameters essential to the dynamics given by Eqs. (4) and (5),

$$\chi_0=\omega_{\beta0}\xi_0\sigma_z/c\,\eta, \quad \chi_1=\omega_{\beta0}\xi_1\sigma_z/c\,\eta, \tag{6}$$

$$\Upsilon=\pi N r_0\langle W_\perp\rangle c^2/8\gamma C\omega_{\beta0}\omega_s, \tag{7}$$

where χ_0 (χ_1) is the dc (ac) phase shift between the head and tail of a bunch, $\langle W_\perp\rangle=(1/N)\int_{-\infty}^{\infty}dz'\rho(z')W(z-z')$. The parameter Υ is approximately the ratio of betatron tune shift to the synchrotron tune. It is well known [9,12] that, when $\chi_1=0$, the SHT instability occurs when $\Upsilon\gtrsim1$.

A. Eigenmode equation

We now present a linearized Vlasov analysis of a many-particle system. We first write down expressions for the dynamical variables in the four-dimensional phase space $(z,y;\delta,y')$, in terms of the action-angle variables. The longitudinal dynamical variables are shown in Eq. (5), and the transverse dynamical variables are

$$y=r_y \cos \phi_y, \quad y'=-\frac{\omega_{\beta0}}{c}r_y \sin \phi_y, \tag{8}$$

where $\phi_{(z,y)}=\omega_{(s,\beta0)}s/c$. The linearized Vlasov equation can then be expressed as

$$-i\frac{\Omega}{c}\psi_1+\frac{\omega_{\beta0}}{c}\frac{\partial\psi_1}{\partial\phi_y}+\frac{\omega_s}{c}\frac{\partial\psi_1}{\partial\phi_z}+\frac{F_y(z,s)}{E}\frac{\partial\psi_0}{\partial y'}\approx0, \tag{9}$$

where the distribution function is expanded as $\psi=\psi_0+\psi_1\exp(-i\Omega s/c)$, and Ω is the mode frequency. Equation (9) can be solved by [9] (1) decomposition of the unperturbed and perturbed distribution functions as

$$\psi_0=\psi_{0z}(r_z)\psi_{0y}(r_y), \quad \psi_1=\psi_{1z}(r_z,\phi_z)\psi_{1y}(r_y,\phi_y); \tag{10}$$

(2) assuming

$$\psi_{1y}(r_y,\phi_y)=-\langle y\rangle\psi_{0y}'(r_y)e^{i\phi_y}, \tag{11}$$

which describes the transverse dipole oscillation, where $\langle y\rangle$ is the beam centroid of transverse motion; and (3) using a linear model of the deflecting force given by

$$F_y(z,s)=i\frac{\langle y\rangle e^2}{CT_0}e^{-i\Omega s/c}\sum_p \tilde{\rho}_1(\omega_p)Z_1^{\perp}(\omega_p)e^{i\omega_p z/c}, \tag{12}$$

where $\omega_p=p\omega_0+\Omega$, $\omega_0=c/R$ is the revolution angular frequency,

$$\rho_1(z)=\int d\delta\ \psi_{1z}(r_z,\phi_z), \tag{13}$$

$\int dz\ d\delta\psi_{0z}=N$, and $Z_1^{\perp}(\omega)$ is the total transverse impedance of the ring. Note that Eq. (12) can be obtained by a Fourier transform of the right-hand side of Eq. (4). The linearized Vlasov equation, including the chromatic term, now becomes

$$\left[i(\Omega-\omega_{\beta 0})\psi_{1z}-\omega_s\frac{\partial\psi_{1z}}{\partial\phi_z}\right]e^{i\phi_y}-\frac{c^2r_0\psi_{0z}}{2\gamma\omega_{\beta 0}CT_0}$$

$$\times(e^{i\phi_y}-e^{-i\phi_y})\sum_p \tilde{\rho}_1(\omega_p)Z_1^{\perp}(\omega_p)e^{i\omega_p r_z\cos\phi_z/c}=0, \tag{14}$$

where ψ_{1z} has an implicitly infinite number of oscillation modes.

To solve the oscillation frequency for each eigenmode of ψ_{1z}, we Fourier expand the longitudinal perturbed distribution function as

$$\psi_{1z}=\sum_l \alpha_l R_l(r_z)e^{i(l\phi_z-\Phi)}, \tag{15}$$

where

$$\Phi=\omega_{\beta 0}\int\frac{ds}{c}\xi\delta=-\frac{\omega_{\xi 0}}{c}r_z\cos\phi_z-\frac{\omega_{\xi 1}}{4c}r_z\cos(2\phi_z), \tag{16}$$

$\omega_{\xi(0,1)}=\omega_{\beta 0}\xi_{(0,1)}/\eta$, $R_l(r_z)$ is the radial eigenfunction, and l is the azimuthal mode index. We emphasize that, in this paper, the radial and the azimuth refer, respectively, to the amplitude (r_z) and phase (ϕ_z) in the longitudinal phase space [cf. Eq. (5)].

Note that, in deriving Eq. (16), we used $\xi=\xi_0+\xi_1\cos\phi_z$, such that the tune spread generated by the in-phase oscillation between the chromaticity modulation and the energy oscillation does not contribute to the chromatic phase advance Φ in Eq. (16). Here we attempt to find the growth rate of the HT instability, neglecting the effect of resonance that causes Landau damping.

To obtain the eigenmode equation for the lth mode, we apply

$$\frac{1}{(2\pi)^2}\int_0^{2\pi}d\phi_z e^{-il'\phi_z+i\Phi}\int_0^{2\pi}d\phi_y e^{-i\phi_y} \tag{17}$$

on both sides of Eq. (14), in which ψ_{1z} is replaced by Eq. (15); we then have

$$(\Omega^{(l)}-\omega_{\beta 0}-l\omega_s)\alpha_l R_l(r_z)$$

$$=i\frac{4\omega_s\Upsilon}{\pi NW_{\perp}T_0}\psi_{0z}(r_z)\sum_q \tilde{\rho}_1(\omega_q)Z_1^{\perp}(\omega_q)I_l(\omega_q), \tag{18}$$

where $\omega_q=q\omega_0+\omega_{\beta 0}+l\omega_s$, by using the generating functions of Bessel functions

$$e^{\pm ix\cos\phi}=\sum_m i^{\pm m}J_m(x)e^{im\phi}, \tag{19}$$

$$e^{\pm ix\sin\phi}=\sum_m i^{\mp m}J_m(x)e^{im\phi}e^{im\pi/2}, \tag{20}$$

and Eq. (13),

$$I_l(\omega_q)=\langle e^{-il\phi_z+i(\omega_q-\omega_{\xi 0})(r_z/c)\cos\phi_z-i\omega_{\xi 1}(r_z/4c)\cos(2\phi_z)}\rangle_{\phi_z}$$

$$=i^l G_q^{(l)*}\left(\frac{\omega_{\xi 1}}{4c}r_z,\frac{\omega_q-\omega_{\xi 0}}{c}r_z\right), \tag{21}$$

$$\tilde{\rho}_1(\omega_q)=\int dz e^{-i\omega_q z/c}\rho_1(z)$$

$$=2\pi\frac{\omega_s}{c\eta}\sum_{l'}i^{-l'}\alpha_{l'}\int_0^{\infty}dr_z' r_z' R_{l'}(r_z')$$

$$\times G_q^{(l')}\left(\frac{\omega_{\xi 1}}{4c}r_z',\frac{\omega_q-\omega_{\xi 0}}{c}r_z'\right), \tag{22}$$

$$G_q^{(l)}\left(\frac{\omega_{\xi 1}}{4c}r_z,\frac{\omega_q-\omega_{\xi 0}}{c}r_z\right)$$

$$=\sum_m i^{-m}J_m\left(\frac{\omega_{\xi 1}}{4c}r_z\right)J_{2m+l}\left(\frac{\omega_q-\omega_{\xi 0}}{c}r_z\right), \tag{23}$$

and the bracket $\langle\ \rangle$ means a longitudinal phase-space average: $\langle\rangle=\langle\rangle_{r_z}\langle\rangle_{\phi_z}$,

$$\langle f(r_z)\rangle_{r_z}=\frac{\int_0^{\infty}dr_z r_z f(r_z)\psi_{0z}(r_z)}{\int_0^{\infty}dr_z r_z\psi_{0z}(r_z)}, \tag{24}$$

$$\langle f(\phi_z)\rangle_{\phi_z}=\frac{1}{2\pi}\int_0^{2\pi}d\phi_z f(\phi). \tag{25}$$

Note that, when $\xi_1=0$, Eq. (18) is the eigenmode equation for the case of a constant chromaticity [9], where $G_q^{(l)}(x_q-x_0)=J_l(x_q-x_0)$.

B. Degenerate radial mode

The eigenmode equation shown in Eq. (18) can be simplified by assuming a hollow distribution,

$$\psi_{0z}(r_z)=\frac{N\eta c}{2\pi\omega_s\hat{z}}\delta(r_z-\hat{z}), \tag{26}$$

where the radial perturbation occurs only on the surface of a δ shell in longitudinal phase space, i.e., $R_l(r_z) \propto \delta(r_z - \hat{z})$. For the zero-order perturbation, $\alpha_{ll'}^{(l)} = \delta_{ll'}$, $\Omega^{(l)} = \omega_{\beta 0} + l\omega_s$. The mode frequency of the first-order perturbation, for the lth mode, is then [cf. Eqs. (18)–(23)]

$$(\Omega^{(l)} - \omega_{\beta 0} - l\omega_s) = i \frac{4\omega_s \Upsilon}{\pi W_\perp T_0} \sum_q Z_1^\perp(\omega_q) \left| G_q^{(l)}\left(\frac{\chi_1}{4}, \chi_q - \chi_0\right)\right|^2, \tag{27}$$

where $\chi_q = \omega_q \hat{z}/c = (q\omega_0 + \omega_{\beta 0} + l\omega_s)\hat{z}/c$, and $\chi_{(0,1)} = \omega_{\xi(0,1)}\hat{z}/c$.

With Eq. (27), we can now find the growth rate, which is the imaginary part of the mode frequency. For a broadband impedance, the growth rate of the head-tail instability per synchrotron period, given in terms of the imaginary part of the mode frequency, is then

$$1/\tau_s^{(l)} = -\frac{4\Upsilon}{\pi} \int d\omega_q \widetilde{Z}_r(\omega_q) \left| G_q^{(l)}\left(\frac{\chi_1}{4}, \chi_q - \chi_0\right)\right|^2, \tag{28}$$

where $Z_1^\perp(\omega_q) = -W_\perp \widetilde{Z}(\omega_q) = -W_\perp[\widetilde{Z}_r(\omega_q) + i\widetilde{Z}_i(\omega_q)]$, and Σ_q has been replaced by $\int \omega_q/\omega_0$. In Fig. 1, we show the growth rate of the impedance corresponding to a uniform wake function, where [9]

$$\widetilde{Z}(\omega_q) = \frac{1}{\omega_q} - i\pi\delta(\omega_q), \tag{29}$$

and the growth rate of the impedance of the broadband resonator model, where

$$\widetilde{Z}(\omega_q) = \frac{1}{2\omega_q \widetilde{z}[1 + i(1/\widetilde{\omega} - \widetilde{\omega})]}, \tag{30}$$

$Q = 1$, $\widetilde{z} = \hat{z}/b$, $\widetilde{\omega} = \omega_q/\omega_R$, $\omega_R = c/b$, and $W_\perp = -2c\hat{z}R_s/b^3$. Note that impedances for the broadband resonator model and the uniform-wake model give a similar dependence of the growth rates on χ_0 and χ_1 (cf. Fig. 1). In the resonator model, a longer bunch would scale down the growth rate of the HT instability. In the uniform-wake model, the growth rate is independent of σ_z. To illustrate the effectiveness of damping mechanism due to χ_1, we will employ Eq. (29) as the function of impedance in the following analysis and simulations.

Note that $1/\tau_s^{(l)} = 0$ when $\chi_0 = 0$, since $\widetilde{Z}_r(\omega_q)$ is odd in ω_q. As emphasized, the ac part of the chromaticity alone does not cause the HT instability. The growth rate for the uniform-wake impedance can be approximated as

$$1/\tau_s^{(l)} \approx \frac{16\Upsilon\chi_0}{\pi} J_0^2\left(\frac{\chi_1}{4}\right) \int_0^\infty \frac{d\chi_q}{\chi_q} J_l(\chi_q) J_l'(\chi_q) \approx \frac{32\Upsilon\chi_0}{\pi^2(4l^2-1)} J_0^2\left(\frac{\chi_1}{4}\right) \tag{31}$$

up to the first order of χ_0, where the terms of $m \neq 0$ in $G_q^{(l)}$ [cf. Eq. (23)] are ignored. The growth rate is obviously decreased by the ac amplitude χ_1. When $\chi_1 = 0$, Eq. (31) reduces to the well-known [4,9] formula $1/\tau_s^{(l)} = 32\Upsilon\chi_0/\pi^2(4l^2-1)$.

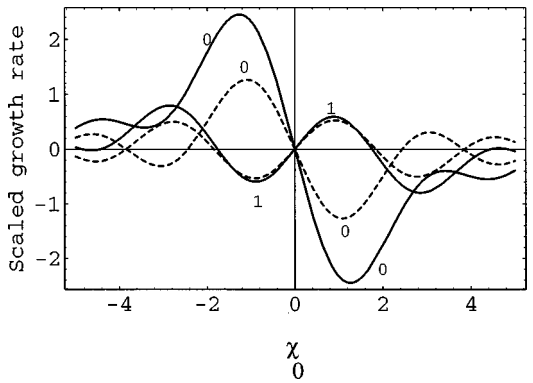

FIG. 1. Scaled growth rate $1/\tau_s^{(l)}/\Upsilon$ of a hollow beam due to the impedances of a uniform-wake (solid line) and a broadband resonator model (dashed line), when $\chi_1 = 0$ and $\widetilde{z} = 0.1$. Curves are labeled by the azimuthal mode index l. See Eqs. (6) and (7) for definitions of χ_0, χ_1, and Υ.

C. Radial modes

When considering realistic particle distributions, the radial eigenfunctions $R_l(r_z)$ are no longer degenerate. In this section, we assume a Gaussian longitudinal distribution, i.e.,

$$\psi_{0z}(r_z) = \frac{N\eta c}{2\pi\sigma_z^2\omega_s} e^{-r_z^2/2\sigma_z^2}, \tag{32}$$

and that the mode frequency shift $\Delta\Omega^{(l)}$ is smaller than ω_s, so that the modes $\Omega^{(l)}$ do not couple. The issues of azimuthal mode coupling will be briefly discussed later. The eigenmode equation, for the uncoupled lth mode, is a modified form of Sacherer's integral equation,

$$\left(\frac{\Omega^{(l)} - \omega_{\beta 0}}{\omega_s} - l\right) R_l(r_z) = W(r_z) \int_0^\infty dr_z' r_z' R_l(r_z') K_l(r_z, r_z'), \tag{33}$$

where

$$W(r_z) = \frac{\omega_s}{N\eta c}\psi_{0z}(r_z) = \frac{1}{2\pi\sigma_z^2} e^{-r_z^2/2\sigma_z^2}, \tag{34}$$

and the kernel of the integral equation is given by

$$K_l(r_z, r_z') = -i\frac{8\Upsilon}{T_0} \sum_q \widetilde{Z}(\omega_q) G_q^{(l)}\left(\frac{\omega_{\xi 1}}{4c} r_z, \frac{\omega_q - \omega_{\xi 0}}{c} r_z\right) \times G_q^{(l)*}\left(\frac{\omega_{\xi 1}}{4c} r_z', \frac{\omega_q - \omega_{\xi 0}}{c} r_z'\right). \tag{35}$$

Introducing an orthonormal complete set $\mathbf{e}_j^{(l)}(r_z)$ defined by

$$\int_0^\infty dr_z r_z W(r_z) \mathbf{e}_j^{(l)}(r_z) \mathbf{e}_{j'}^{(l)}(r_z) = \delta_{jj'}, \tag{36}$$

the eigenfunction can be expanded as

$$R_l(r_z)=W(r_z)\sum_{j=0}^{\infty} a_j \mathbf{e}_j^{(l)}(r_z). \tag{37}$$

For a Gaussian unperturbed distribution the weight function $W(r_z)$ [cf. Eq. (34)] has the orthonormal basis $\mathbf{e}_j^{(l)}(r_z)$ given by [13]

$$\mathbf{e}_j^{(l)}(r_z)=\left(\frac{2\pi j!}{(l+j)!}\right)^{1/2}\left(\frac{r_z}{\sqrt{2}\sigma_z}\right)^l L_j^{(l)}\left(\frac{r_z^2}{2\sigma_z^2}\right), \tag{38}$$

where $L_j^{(l)}$ are the Laguerre polynomials. We now apply

$$\int_0^{\infty} dr_z r_z \mathbf{e}_j^{(l)}(r_z) \tag{39}$$

to both sides of Eq. (33). The integral equation becomes an eigenvalue system,

$$\left|\left(\frac{\Omega^{(l)}-\omega_{\beta 0}}{\omega_s}-l\right)\mathbf{I}-\mathbf{M}^{(l)}\right|=0, \tag{40}$$

where $\mathbf{I}$ is an identity matrix,

$$\mathbf{M}_{jj'}^{(l)}=-i\frac{8\Upsilon}{T_0}\sum_q \tilde{Z}(\omega_q) g_{lj}(\omega_{\xi 1},\omega_q-\omega_{\xi 0}) \times g_{lj'}^{*}(\omega_{\xi 1},\omega_q-\omega_{\xi 0}), \tag{41}$$

and

$$g_{lj}(\omega_{\xi 1},\omega_q-\omega_{\xi 0})=\int_0^{\infty} dr_z r_z W(r_z)\mathbf{e}_j^{(l)}(r_z) \times G_q^{(l)}\left(\frac{\omega_{\xi 1}}{4c}r_z,\frac{\omega_q-\omega_{\xi 0}}{c}r_z\right). \tag{42}$$

Note that the meaning of g_{lj} is related to the frequency spectrum of the (l,j) mode of the perturbed beam density, since [cf. Eqs. (22), (23), and (42)]

$$\tilde{\rho}_1(\omega_q)=2\pi\frac{\omega_s}{c\eta}\sum_l\sum_{j=0} i^{-l}\alpha_l a_j g_{lj}(\omega_{\xi 1},\omega_q-\omega_{\xi 0}). \tag{43}$$

The eigenvalues need to be solved by diagonalization of the infinite-dimensional matrix $\mathbf{M}^{(l)}$. Note that, when $\chi_0=\chi_1=0$, the number of azimuthal and radial nodes in the longitudinal phase space are l and j, respectively. When there is the chromaticity, more ripples would appear in the longitudinal phase space. To achieve a qualitative description of the eigenmodes, we now focus only on the dominant radial mode, where $j=0$. Using Eqs. (23), (34), and (38), for the integral in Eq. (42), in which $L_0^{(l)}(x^2)=1$, we have [13], for the $(l,j)=(l,0)$ mode,

$$g_{l0}(x_1,x_q-x_0) =\frac{1}{\sqrt{2\pi l!}}\sum_{m=0}(2-\delta_{m0})\left(-i\frac{x_1}{4}\right)^m \times\frac{(x_q-x_0)^{2m+l}}{(2m+l)!}\sum_{p=0}(-1)^p \times\frac{\Gamma(p+l+3m/2+1)}{p!\Gamma(p+m+1)}\left(\frac{x_1}{4}\right)^{2p} \times {}_2F_1\left[-p,-m-p;2m+l+1;\left(\frac{x_q-x_0}{x_1/4}\right)^2\right], \tag{44}$$

where $x_{(0,1)}=\omega_{\xi(0,1)}\sigma_z/\sqrt{2}c$, $x_q=\omega_q\sigma_z/\sqrt{2}c$, δ_{m0} is the Kronecker delta, and ${}_2F_1(a,b;c;x)$ is the hypergeometric function. Note that $x_{(0,1,q)}=\chi_{(0,1,q)}/\sqrt{2}$. The beam spectra $|g_{l0}(\chi_q)|^2$ are shown in Fig. 2. It can be seen that, the center of spectra is shifted by an amount of χ_0, and, with a large enough χ_1, the spectral amplitudes are suppressed for all azimuthal modes. This implies that, besides the additional incoherent tune spread due to χ_1 which causes Landau damping, the HT instability induced by χ_0 is further suppressed by χ_1, although the latter effect is much less effective than the first one, as will be seen in Sec. III.

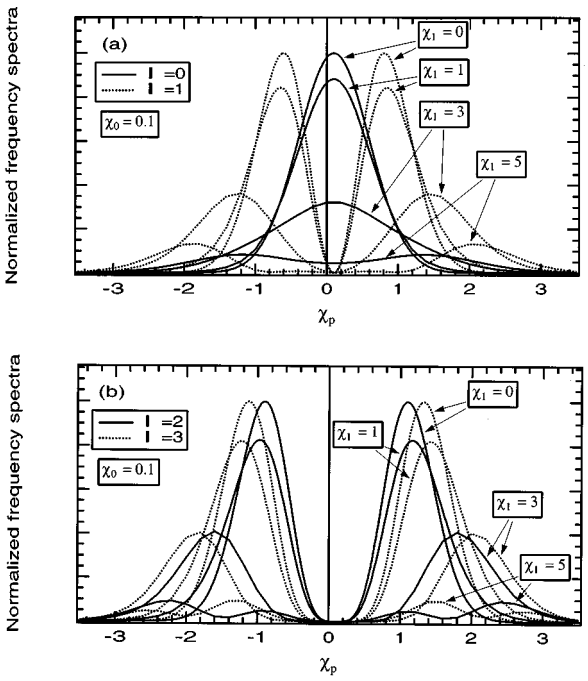

FIG. 2. Normalized frequency spectra $|g_{l0}(\chi_q)|^2$ of a Gaussian beam, when $\chi_0=0.1$, (a) $l=0$ and 1, and (b) $l=2$ and 3. See Eq. (6) for definitions of χ_0 and χ_1.

The beam spectrum $g_{l0}(0,\chi_q-\chi_0)$ reduces to the spectrum of the dc case when $\xi_1=0$:

$$g_{l0}(\chi_q-\chi_0)=\frac{1}{\sqrt{2\pi l!}2^{l/2}}(\chi_q-\chi_0)^l e^{-(\chi_q-\chi_0)^2/2}. \tag{45}$$

The mode frequency can now be approximated for the dominant radial mode of a Gaussian beam, as

$$\Omega^{(l)}-\omega_{\beta 0}-l\omega_s\simeq -i\frac{8\Upsilon\omega_s}{T_0}N_g^{(l)}\tilde{Z}_{\mathrm{eff}}^{(l)}, \tag{46}$$

where

$$N_g^{(l)}=\sum_q |g_{l0}(\chi_1,\chi_q-\chi_0)|^2, \tag{47}$$

and the effective impedance is

$$\tilde{Z}_{\rm eff}^{(l)}=[N_g^{(l)}]^{-1}\sum_q \tilde{Z}(\omega_q)|g_{l0}(\chi_1,\chi_q-\chi_0)|^2. \tag{48}$$

When $\chi_1<1$, one can approximate the beam spectrum by

$$|g_{l0}(\chi_1,\chi_q-\chi_0)|^2\approx\frac{1}{2\pi l!2^l}(\chi_q-\chi_0)^{2l}e^{-(\chi_q-\chi_0)^2}J_0^2\left(\frac{\chi_1}{4}\right). \tag{49}$$

For simplicity, instead of using the exact representation of the beam spectrum shown in Eq. (44), we use the approximate form of Eq. (49) in the following study, for the case of $\chi_1<1$. In this way, for a broadband impedance, the growth rate per synchrotron period is simply

$$\begin{aligned}1/\tau_s^{(l)}&\simeq -8\Upsilon\int d\omega_q\tilde{Z}_r(\omega_q)|g_{l0}(\chi_1,\chi_q-\chi_0)|^2\\&=-8\Upsilon N_l\ {\rm Re}[\tilde{Z}_{\rm eff}^{(l)}],\end{aligned} \tag{50}$$

where, for a Gaussian beam,

$$N_l=\int d\omega_q|g_{l0}|^2\approx\frac{\Gamma(l+1/2)}{\pi l!2^{l+1}}\frac{c}{\sigma_z}J_0^2\left(\frac{\chi_1}{4}\right). \tag{51}$$

The coherent tune shift is given by the real part of the mode frequency. For a uniform-wake impedance [cf. Eq. (29)], we have

$$2\pi\ {\rm Re}[\Delta\nu^{(l)}]\approx-\frac{4\Upsilon}{l!2^l}\nu_s\chi_0^{2l}e^{-\chi_0^2}J_0^2\left(\frac{\chi_1}{4}\right), \tag{52}$$

where $\Delta\nu^{(l)}=(\Omega^{(l)}-\omega_{\beta 0})/\omega_0-l\nu_s$, $\nu_s=\omega_s/\omega_0$; and the growth rates of the two fundamental modes are approximately

$$1/\tau_s^{(0)}\approx-4\Upsilon\ {\rm Erf}_i(\chi_0)e^{-\chi_0^2}J_0^2\left(\frac{\chi_1}{4}\right), \tag{53}$$

and

$$1/\tau_s^{(1)}\approx\sqrt{\pi}\Upsilon\chi_0 L_{1/2}^{(-1/2)}(\chi_0^2)e^{-\chi_0^2}J_0^2\left(\frac{\chi_1}{4}\right), \tag{54}$$

where $1/\tau_s^{(l)}=2\pi\,{\rm Im}[\Delta\nu^{(l)}]/\nu_s$, ${\rm Erf}_i(x)=-i\ {\rm Erf}(ix)$, and ${\rm Erf}(x)$ is the error function. One can see that, when $\chi_0=0$, the growth rate of HT instability is zero, even when $\chi_1\neq 0$. This means that the varying part of the chromaticity does not cause instability.

Figure 3 show the real and imaginary parts of the coherent tune shifts for $l=0$ and $l=1$. When $\chi_0\ll 1$, the growth rates can be further approximated by using ${\rm Erf}(\chi_0)\approx 2\chi_0/\sqrt{\pi}$, $L_{1/2}^{(-1/2)}(\chi_0^2)\approx 2/\pi$. For a uniform-wake impedance, and $\chi_1<1$, we recapitulate the growth rates in Table I, when $\chi_0\ll 1$.

Simulations agree very well with Eq. (53) for the damping and growth rates of the $l=0$ mode of a Gaussian beam.

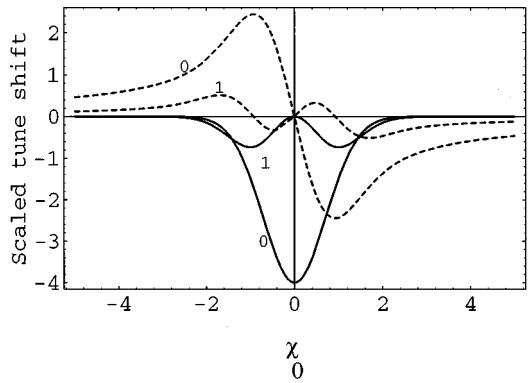

FIG. 3. Scaled coherent tune shift of a Gaussian beam due to the impedance of Eq. (29) vs χ_0, when $\chi_1=0$, and where the solid (dashed) lines are the real (imaginary) part of $2\pi\Delta\nu^{(l)}/\nu_s\Upsilon$. Curves are labeled by the azimuthal mode index l. See Eqs. (6) and (7) for definitions of χ_0, χ_1, and Υ.

Figure 4 shows examples of the bunch centroid motion of a Gaussian beam, where the evolution of the envelope agrees very well with the theory's prediction. In other words, the imaginary part of the coherent tune shift calculated is confirmed by simulations.

When the SHT effect is prominent, i.e., when Υ is close to 1, the azimuthal mode coupling is likely to occur. Examination of Eqs. (52), (53), and (54) shows that both the real and imaginary parts of the coherent tune shift of the $(l,0)$ mode are approximately reduced by $J_0^2(\chi_1/4)$. Even before solving the matrix of infinite dimension, or including the Landau damping, this suggests that the SHT threshold can be raised by a large value of χ_1.

The most important results in this section are Eqs. (52), (53), and (54), which are the real and imaginary parts of the tune shift of a Gaussian beam with the model impedance of Eq. (29). These results will be used in Sec. III.

III. LANDAU DAMPING

In this section, we include in the linearized Vlasov analysis the incoherent tune spread induced by the varying chromaticity. We present an approximate stability criterion, a rigorous criterion using the dispersion relation, and comparisons with simulation results.

Let us first estimate the incoherent chromatic tune spread due to ξ_1:

$$\sigma_\nu\approx\nu_{\beta 0}\xi_1\sqrt{\langle(\delta\ \sin\ \phi_z)^2\rangle}\approx\sqrt{3/8}g_\sigma\nu_{\beta 0}\xi_1\sigma_\delta, \tag{55}$$

TABLE I. Comparisons of the geometric factor of the growth rate of the HT instability, for a bunched beam with a hollow distribution and with a Gaussian distribution, when $\chi_0\ll 1$. A uniform-wake impedance is assumed, and the effect of Landau damping is not included.

	$[\tau_s^{(l)}\chi_0\Upsilon J_0^2(\chi_1/4)]^{-1}$	
	hollow	Gaussian
$l=0$	-3.242	-4.514
$l=1$	1.081	1.128

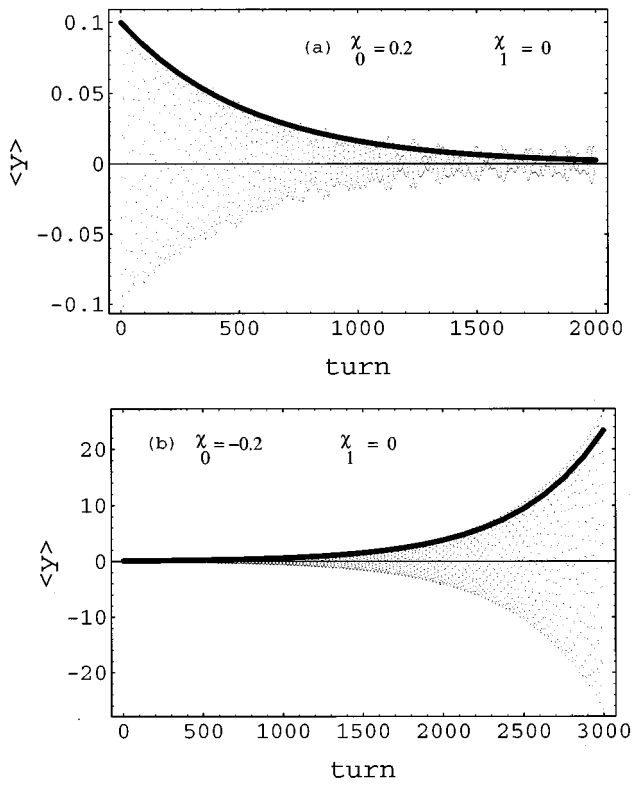

FIG. 4. Multiparticle simulation results showing the motion of bunch centroid of a Gaussian beam, when $\chi_1=0$, $\Upsilon=0.22$, (a) $\chi_0=+0.2$, and (b) $\chi_0=-0.2$. The solid lines are where, according to Eq. (53), $\langle y\rangle[\text{turn}]=0.1\exp[\nu_s(\text{turn})/\tau_s^{(0)}]$. See Eqs. (6) and (7) for definitions of χ_0, χ_1, and Υ.

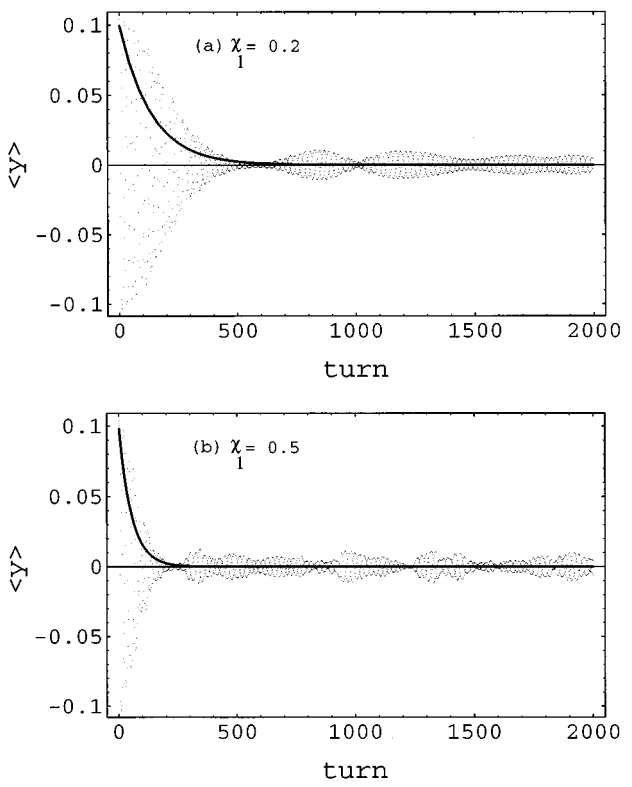

FIG. 5. Multiparticle simulation results showing decoherence of the centroid motion of a Gaussian beam, when $\Upsilon=0.11$, $\chi_0=0$, (a) $\chi_1=0.2$, and (b) $\chi_1=0.5$. The solid lines are where, according to Eq. (56), $\langle y\rangle[\text{turn}]=0.1\exp[-(\text{turn})/\tau_{\text{dec}}]$. See Eqs. (6) and (7) for definitions of χ_0, χ_1, and Υ.

where $\nu_{\beta 0}=\omega_{\beta 0}/\omega_0$, and $g_\sigma=\sqrt{\langle r_z^2\rangle_{r_z}}/\sigma_z$ is a geometric factor depends on the longitudinal distribution $\psi_{0z}(r_z)$. For a Gaussian distribution, $g_\sigma=1$.

The ac part of the incoherent tune spread contributes to a Landau damping without driving the HT instability [cf. Eqs. (53) and (54)]. The Landau damping rate needs to be solved by the dispersion relation including the tune spread, where the beam frequency spectrum, beam intensity, and impedance are involved. In general, a larger width of the tune spread can give a faster Landau damping [9]. This implies that, within the tolerance of dynamic aperture reduction due to resonance, one can increase the damping rate (by a large enough χ_1) to suppress the HT instability.

The ac part of the incoherent tune spread also contributes to the decoherence. Decoherence is an effect that causes decay of centroid oscillation of an off-centered beam with frequency spread, and is an excitation response to a nonzero initial condition [9,14]. The decoherence rate per turn can be estimated as

$$\tau_{\text{dec}}^{-1}\approx 2\pi\sigma_\nu. \tag{56}$$

In Figs. 5 and 6, we show that, when there is no HT instability ($\chi_0=0$), the approximation for the decoherence rate is confirmed by simulations of a bunched beam traversing an impedance in a storage ring [cf. Appendix B].

A. Approximate stability criterion

With the knowledge of the incoherent tune spread and coherent tune shift, which cause damping and instability, respectively, we can estimate a stability condition. The stability criterion can be estimated by requiring that the incoherent tune spread exceeds the absolute value of the coherent tune shift, that is,

$$\sigma_\nu > |\Delta\nu^{(l)}|. \tag{57}$$

From Eqs. (55) and (46), a general expression for the stability condition is

$$\chi_1 > \frac{8}{\pi}\left(\frac{2}{3}\right)^{1/2}\left(\frac{N_l}{g_\sigma}\right)\Upsilon|\tilde{Z}_{\text{eff}}^{(l)}(\chi_0)|, \tag{58}$$

where the factor $J_0^2(\chi_1/4)$ is neglected. From Eqs. (46), (47), and (49), and Fig. 2, one can see that, without taking into account Landau damping, χ_1 does not significantly reduce the coherent tune shift, unless $\chi_1\gg 1$. Expressed in terms of the accelerator parameters, the approximate stability criterion is

$$\xi_1 > c_l\frac{eI_0|Z_1^{\perp(l)}(\xi_0)|_{\text{eff}}}{E}\left(\frac{R}{\sigma_z}\right)^2\left(\frac{\eta R}{\nu_s\nu_{\beta 0}^2}\right), \tag{59}$$

where $c_l=\sqrt{2/3}\Gamma(l+1/2)/\pi l!2^{l+1}$, and the average current is $I_0=Nec/C$. When $0<\chi_0<1$, the $l=1$ mode is usually the dominant unstable mode, and $c_1=0.058$. In contrast, when

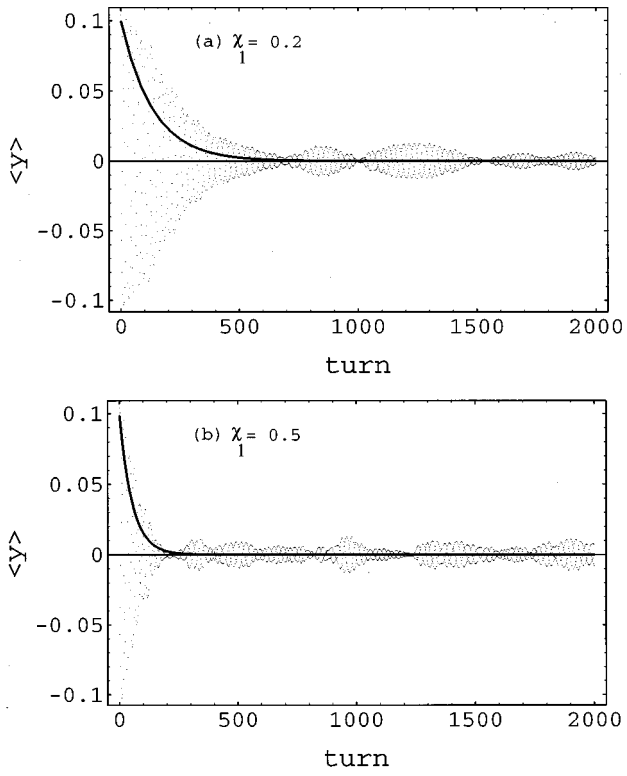

FIG. 6. Multiparticle simulation results showing the decoherence of the centroid motion of a Gaussian beam, when $\Upsilon = 0.328$, $\chi_0 = 0$, (a) $\chi_1 = 0.2$, and (b) $\chi_1 = 0.5$. The solid lines are where, according to Eq. (56), $\langle y \rangle[\text{turn}] = 0.1 \exp[-(\text{turn})/\tau_{\text{dec}}]$. See Eqs. (6) and (7) for definitions of χ_0, χ_1, and Υ.

$-1 < \chi_0 < 0$, the $l = 0$ mode is the dominant unstable mode, and $c_0 = 0.23$. Note that, as the dimensionality of $Z_1^{\perp}$ is Ω/m, both sides of Eq. (59) are dimensionless.

As an example, consider a Gaussian beam distribution, an impedance function $\tilde{Z} = 1/\omega_q - i\pi\delta(\omega_q)$, and $\chi_0 = 0.2$, the stability criterion [cf. Eq. (58)] predicts that the $l = 0$ mode is stabilized if $\chi_1 > \Upsilon$, and the $l = 1$ mode is stabilized if $\chi_1 > 0.058\Upsilon$. In Figs. 7 and 8, we show the growth of the bunch centroid, rms size, and rms emittance due to the HT instability, and its stabilization by various amounts of χ_1. The value of χ_1 needed to stabilize the bunch centroid motion is approximately consistent with the estimated criterion of Eq. (58). In Fig. 8, the bunch centroid motion is initially dominated by the $l = 0$ mode, which is a damping mode when $\chi_0 > 0$ [cf. Figs. 3 and 4]; the higher-order unstable modes cause the growth of averaged bunch center after the initial damping. The varying chromaticity, nonetheless, Landau damps all the higher-order unstable modes when χ_1 is larger than the threshold estimated in Eq. (58). Note that the emittance growth is much slower than the initial centroid damping (cf. Fig. 8). This is a result of the growth rates of the unstable higher-order modes ($l \geq 1$) being much smaller than the damping rate of the ($l = 0$) mode, e.g., $\tau_s^{-1}(l = 0) \approx -4\tau_s^{-1}(l = 1)$, when $\chi_0 \ll 1$ (cf. Table I).

Equation (58) is usually sufficient for estimating the threshold for bunch centroid motions. An improved stability criterion, useful for estimating the threshold for a growth of the emittance, can be derived by incorporating the incoherent tune spread in the Vlasov analysis. In doing so, one needs to include the damping mode by the method of singular eigenfunction expansion, and solve the dispersion relation [15]. The basic derivations are formulated in Sec. III B.

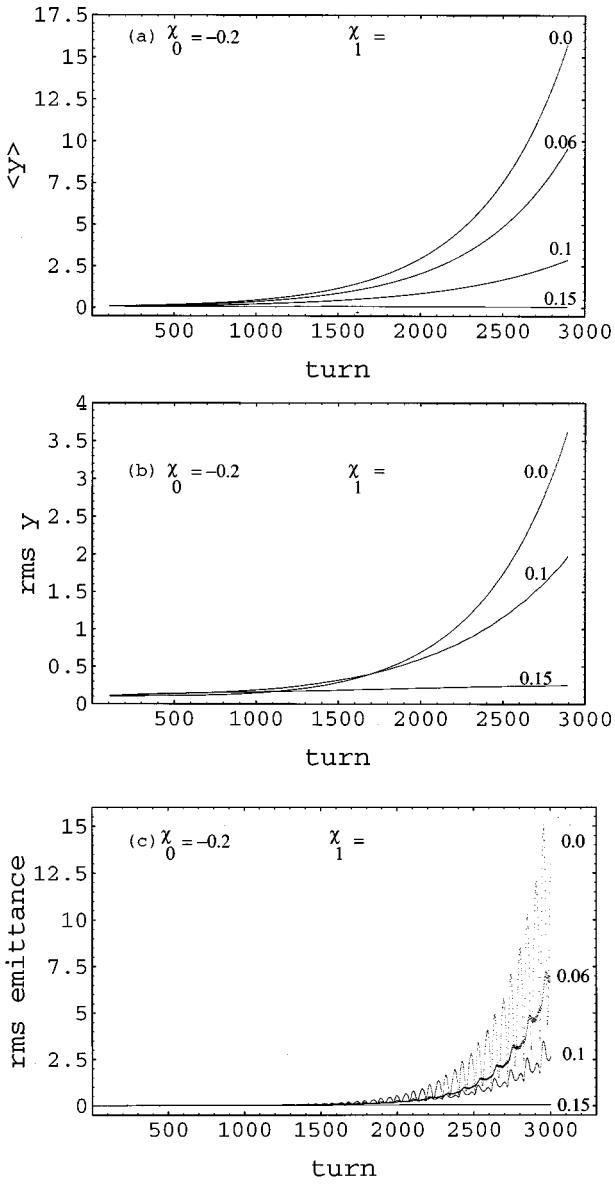

FIG. 7. Multiparticle simulation results showing stabilization of the HT motions of (a) the centroid, (b) the rms size, and (c) the rms emittance of a Gaussian beam by χ_1, when $\chi_0 = -0.2$ and $\Upsilon = 0.22$. The estimated stability threshold for the $l = 0$ mode, according to Eq. (58), is $\chi_1 \geq 0.22$. See Eqs. (6) and (7) for definitions of χ_0, χ_1, and Υ.

B. Singular eigenfunction expansion

In this section, we use the method of singular eigenfunction expansion [15] to include the Landau damping in the Sacherer equation. We first rederive the betatron phase advance, when $\xi = \xi_0 + \xi_1 \sin \phi_z$,

$$\Phi_\beta = \int \frac{ds}{c}\omega_\beta(\delta) = \frac{\omega_{\beta 0}}{c}s + \frac{\omega_{\beta 0}}{c}\int ds\ \xi\delta = \phi_\beta + \Phi, \tag{60}$$

where $\phi_\beta = \phi_y + S_1\phi_z r$,

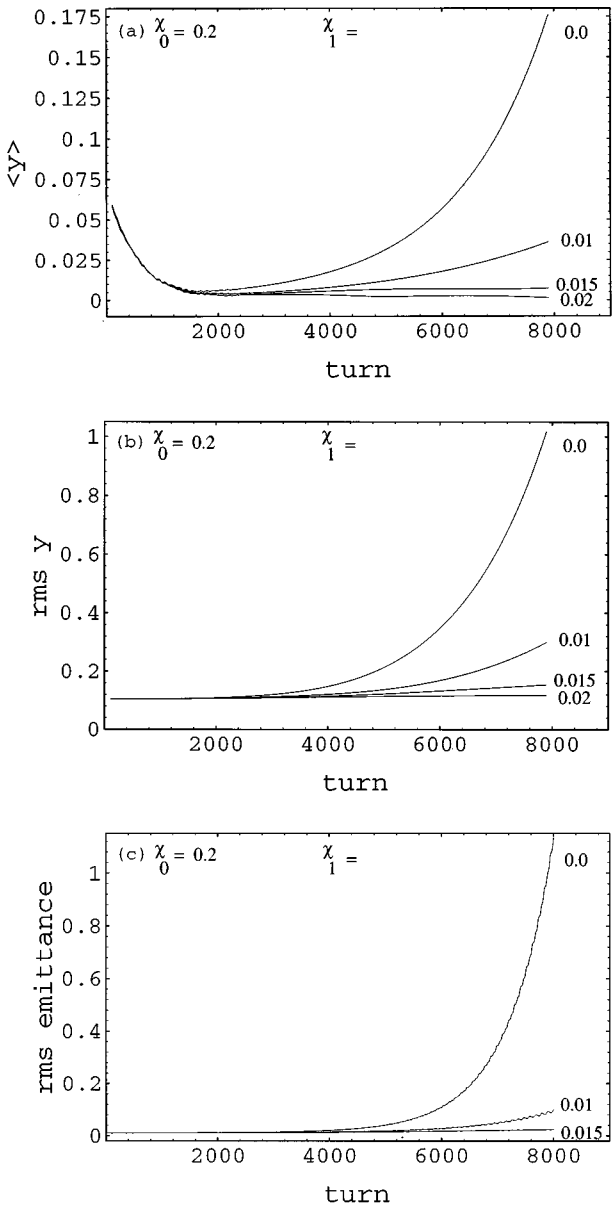

FIG. 8. Multiparticle simulation results showing stabilization of the HT motions of (a) the centroid, (b) the rms size, and (c) the rms emittance of a Gaussian beam by χ_1, when $\chi_0=0.2$ and $\Upsilon=0.22$. The estimated stability threshold for the $l=1$ mode, according to Eq. (58), is $\chi_1 \geqslant 0.0127$. See Eqs. (6) and (7) for definitions of χ_0, χ_1, and Υ.

$$\Phi = -\frac{\omega_{\xi 0}}{c} r \cos\phi_z - \frac{\omega_{\xi 1}}{4c} r \sin(2\phi_z), \tag{61}$$

$r_z \rightarrow r$, and $S_1=\omega_{\xi 1}/2c$. The in-phase oscillation between the chromaticity modulation and the energy oscillation generates a tune spread proportional to $S_1 r$. We now rewrite Eq. (33) as

$$R_l(r) = \frac{W(r)}{\nu_l - S_1 r} \int_0^\infty dr' r' R_l(r') K_l(r,r'), \tag{62}$$

where $\nu_l = (\Omega^{(l)} - \omega_{\beta 0})/\omega_s - l = \Delta\nu^{(l)}/\nu_s$, $\omega_{\beta 0} \rightarrow \omega_{\beta 0} + S_1\omega_s r$, and $\nu_l \rightarrow \nu_l - S_1 r$. According to the orthogonality condition defined in Eq. (36), the kernel $K_l(r,r')$ can be expanded as

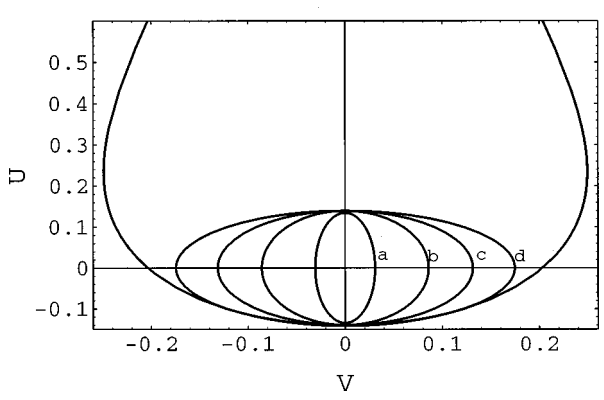

FIG. 9. Stability diagram of a Gaussian beam with the impedance function given by Eq. (29), for the $l=0$ mode. Parameters that label the ellipses are: $(-\chi_0, \Upsilon) =$ (a) (0.2, 0.22), (b) (0.5, 0.28), (c) (0.7, 0.36), and (d) (0.85, 0.45). The outer curve is where $\chi_1=0.7$. See Eqs. (6) and (7) for definitions of χ_0, χ_1, and Υ.

$$K_l(r,r') = \sum_{j,j'} \mathbf{M}^{(l)}_{jj'} \mathbf{e}^{(l)}_j(r) \mathbf{e}^{(l)}_{j'}(r'), \tag{63}$$

where

$$\mathbf{M}^{(l)}_{jj'} = \int_0^\infty dr\ r W(r) \mathbf{e}^{(l)}_j(r) \int_0^\infty dr' r' W(r') \mathbf{e}^{(l)}_{j'}(r') K_l(r,r'). \tag{64}$$

As in Sec. II, we now apply $\int dr\ r \mathbf{e}^{(l)}_j(r)$ on both sides of Eq. (62). The eigenvalue system becomes

$$\delta_{jj'} - \sum_k \alpha^{(l)}_{jk} \mathbf{M}^{(l)}_{kj'} = 0, \tag{65}$$

where

$$\alpha^{(l)}_{jk} = \int dr r \frac{\mathbf{e}^{(l)}_j(r) \mathbf{e}^{(l)}_k(r) W(r)}{\nu_l - S_1 r} = F_{jk}(\nu_l) + i G_{jk}(\nu_l), \tag{66}$$

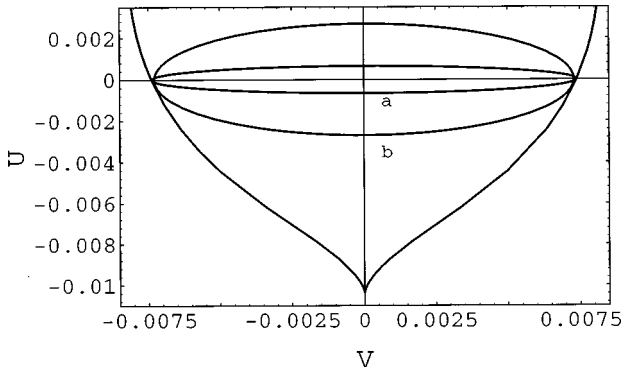

FIG. 10. Stability diagram of a Gaussian beam with the impedance function shown in Eq. (29), for the $l=1$ mode. Parameters that label the ellipses are $(\chi_0, \Upsilon) =$ (a) (0.05, 0.83) and (b) (0.2, 0.22). The outer curve is where $\chi_1=0.026$. See Eqs. (6) and (7) for definitions of χ_0, χ_1, and Υ.

$$F_{jk}(\hat{r}) = -\frac{1}{S_1}\mathrm{P}\int dr r \frac{\mathbf{e}_j^{(l)}(r)\mathbf{e}_k^{(l)}(r)W(r)}{r-\hat{r}},$$

$$G_{jk}(\hat{r}) = -\frac{\pi}{S_1}\hat{r}\mathbf{e}_j^{(l)}(\hat{r})\mathbf{e}_k^{(l)}(\hat{r})W(\hat{r}), \tag{67}$$

$\hat{r}=\nu_l/S_1$, and P is the Cauchy principal value. In Eq. (66), we have used the formula: $1/(r-\hat{r})\rightarrow \mathrm{P}/(r-\hat{r})+i\pi\delta(\hat{r})$. The dispersion relation of the dominant radial mode is

$$\frac{1}{\alpha_{00}^{(l)}} = \mathbf{M}_{00}^{(l)}, \tag{68}$$

or, explicitly,

$$V+iU = \frac{i}{\alpha_{00}^{(l)}} = \frac{i}{F_{00}(\nu_l)+iG_{00}(\nu_l)} = i\mathbf{M}_{00}^{(l)}$$

$$= \frac{8\Upsilon}{2\pi}N_l\{\mathrm{Re}[\tilde{Z}_{\mathrm{eff}}^{(l)}]+i\ \mathrm{Im}[\tilde{Z}_{\mathrm{eff}}^{(l)}]\}, \tag{69}$$

where $V(U)$ is the real (imaginary) part of the $i/\alpha_{00}^{(l)}$, and $i/\alpha_{00}^{(l)}$ is the so called ''beam transfer function'' (BTF). For a Gaussian beam, we have

$$\frac{i}{F_{00}(\nu_0)+iG_{00}(\nu_0)} = \frac{-i\chi_1^2/2}{\sqrt{2\pi}\chi_1 - 2\pi\nu_0 e^{-2\nu_0^2/\chi_1^2}\left[\mathrm{Erf}_i\left(\frac{\sqrt{2}\nu_0}{\chi_1}\right)-i\right]}, \tag{70}$$

and

$$\frac{i}{F_{00}(\nu_1)+iG_{00}(\nu_1)} = \frac{-i\chi_1^4}{\sqrt{2\pi}(\chi_1^3+4\chi_1\nu_1^2) - 8\pi\nu_1^3 e^{-2\nu_1^2/\chi_1^2}\left[\mathrm{Erf}_i\left(\frac{\sqrt{2}\nu_1}{\chi_1}\right)-i\right]}, \tag{71}$$

for the $l=0$ and $l=1$ modes. The real and imaginary parts of the effective impedance are given by [cf. Eqs. (52), (53), and (54)]

$$8\Upsilon N_l\ \mathrm{Re}[\tilde{Z}_{\mathrm{eff}}^{(l)}] = \begin{cases} 4\Upsilon\ \mathrm{Erf}_i(\chi_0)e^{-\chi_0^2}J_0^2\left(\frac{\chi_1}{4}\right) & (l=0) \\ -\sqrt{\pi}\Upsilon\chi_0 L_{1/2}^{(-1/2)}(\chi_0^2)e^{-\chi_0^2}J_0^2\left(\frac{\chi_1}{4}\right) & (l=1), \end{cases} \tag{72}$$

$$8\Upsilon N_l\ \mathrm{Im}[\tilde{Z}_{\mathrm{eff}}^{(l)}] = -\frac{4\Upsilon}{l!2^l}\chi_0^{2l}e^{-\chi_0^2}J_0^2\left(\frac{\chi_1}{4}\right). \tag{73}$$

In Figs. 9 and 10, we show the stability diagrams in the U-V space, when $l=0$ and $l=1$. The curve of the BTF (the outer limit on the U-V plane), is determined by χ_1. The parameters related to the beam intensity and the effective impedance, i.e., Υ and χ_0 [cf. Eqs. (52), (53), and (54)], determine the curve of the inner elliptical circle on the U-V plane. Note that, in drawing the figures, the contribution of $J_0^2(\chi_1/4)$ in the beam spectrum [cf. Eq. (49)] is moved to the left-hand side of the dispersion relation [cf. Eq. (69)].

We find that, the stability limit for the $l=0$ mode is where $\nu_0=0$, i.e., Re(BTF)$=0$. According to the dispersion relation [cf. Eq. (69)], the stability condition is $\Upsilon(l=0) \leqslant 0.31\chi_1 e^{\chi_0^2}$. For the $l=1$ mode, the stability limit is usually given by where $F_{00}=0$, i.e. Im(BTF)$=0$. Unlike the $l=0$ mode, one needs to solve the dispersion relation numerically to obtain the stability condition of the $l=1$ mode. In short, it is the real (imaginary) part of the effective impedance that gives rise to the stability limit, for the $l=1(l=0)$ mode.

Figures 11 and 12 show that the stability area can be

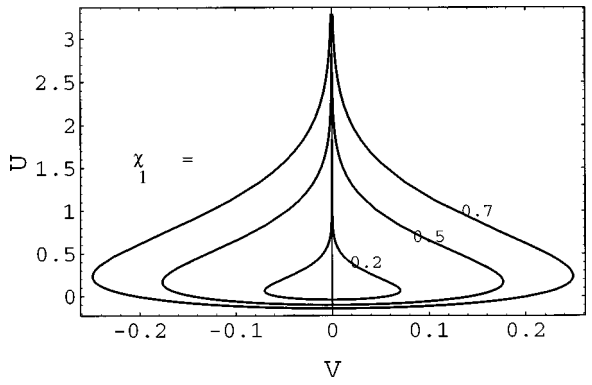

FIG. 11. Stability diagram of a Gaussian beam with the impedance function shown in Eq. (29), for the $l=0$ mode. The stability boundaries are enlarged by χ_1. See Eqs. (6) and (7) for definitions of χ_0, χ_1, and Υ.

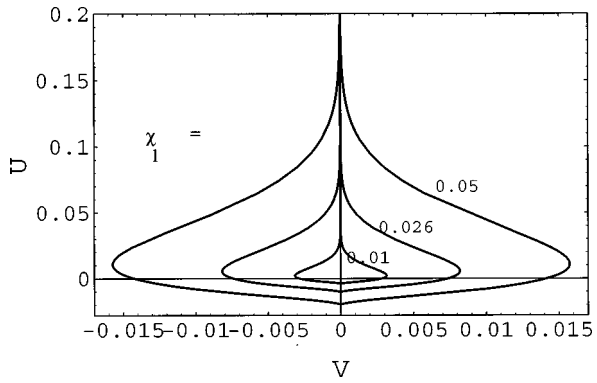

FIG. 12. Stability diagram of a Gaussian beam with the impedance function shown in Eq. (29), for the $l=1$ mode. The stability boundaries are enlarged by χ_1. See Eqs. (6) and (7) for definitions of χ_0, χ_1, and Υ.

enlarged by a larger χ_1, for both the $l=0$ and $l=1$ modes. Equations (70) and (71) show that the left-hand side of the dispersion relation is approximately proportional to χ_1; this implies that the SHT threshold can be enlarged by increasing χ_1.

The multiparticle simulations show that the rms emittance of a Gaussian beam is stabilized when the the value of χ_1 approaches the stability threshold of Eq. (69) [cf. Figs. 13 and 14]. Figure 15 shows that, the results of simulation of the bunch centroid motion agree very well with the approximate stability limits, and the results of emittance growth agree with the exact stability criterion. Compared with the rigorous criterion, to stabilize the bunch's higher moments, such as the rms size and rms emittance, χ_1 usually needs to be larger than the estimate from the approximate criterion [cf. Eq. (58)] by a factor of between 1 and 2. So far, we show the results of when $\Upsilon=0.22$, for other values of Υ, simulations also agree with the theoretical stability criterion (for $\Upsilon<0.2$ such that the SHT effect is not prominent).

As mentioned in previous sections, the varying chromaticity cannot only stabilize the HT effect, but also increase the SHT threshold. Figure 16 shows the simulation results for the stabilization of the SHT instability by a large enough χ_1, when $\Upsilon=1.65$ and $\chi_0=0$. Note that the SHT stability

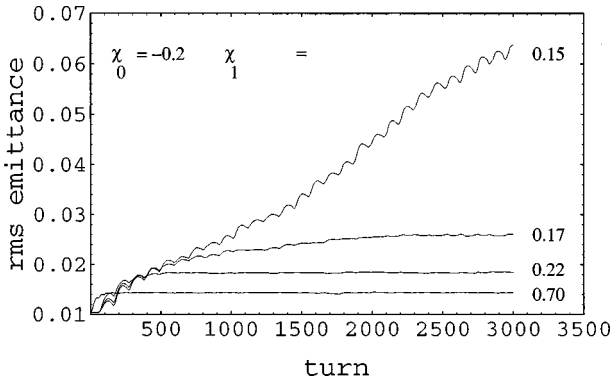

FIG. 13. Multiparticle simulation result showing stabilization of the HT motions of the rms emittance of a Gaussian beam when $\chi_1\to 0.7$—the theoretical stability threshold of the $l=0$ mode [cf. Eq. (69)]. Here $\chi_0=-0.2$, $\Upsilon=0.22$. See Eqs. (6) and (7) for definitions of χ_0, χ_1, and Υ.

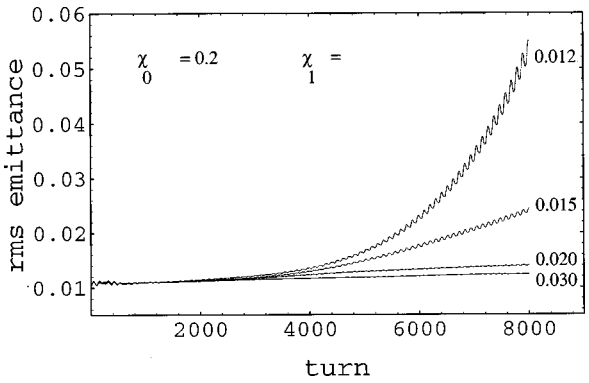

FIG. 14. Multiparticle simulation result showing stabilization of the HT motions of the rms emittance of a Gaussian beam when $\chi_1\to 0.026$—the theoretical stability threshold of the $l=1$ mode [cf. Eq. (69)]. Here $\chi_0=0.2$ and $\Upsilon=0.22$. See Eqs. (6) and (7) for definitions of χ_0, χ_1, and Υ.

threshold, without varying the chromaticity, is $\Upsilon\simeq 1$ (which has been confirmed by simulations). This implies that the limitation of peak current in a storage ring can be increased by varying the chromaticity. The stability criterion derived in this section are in good agreement with the simulation results, and the criterion provides a useful guidance for the implementation of the varying chromaticity scheme.

IV. CONCLUSION

In summary, the chromaticity, causing the head-tail instability in a storage ring without threshold, usually needs to be controlled by sextupoles. We have shown that, by varying the chromaticity, the head-tail instability is suppressed, and a stability threshold is developed. The varying chromaticity contributes to Landau damping without inducing instabilities, one may use an ac amplitude as large as possible (within the tolerance of dynamic aperture reduction) to increase the SHT instability threshold, so as to achieve a higher bunch current in a storage ring. Multiparticle simulations confirmed the estimated decoherence rate, the mode analysis, and the

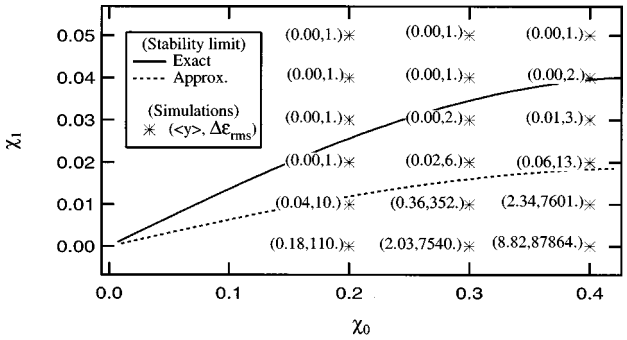

FIG. 15. Stability limits of a Gaussian beam with the impedance function of Eq. (29) for the $l=1$ mode, in the ac (χ_1) vs dc (χ_0) space. Here $\Upsilon=0.22$, $\langle y\rangle$ is the averaged centroid motion at the 8000th turn, $\Delta\varepsilon_{\rm rms}=\varepsilon_{\rm rms}(8000)/\varepsilon_{\rm rms}(0)$, and the approximate and exact stable limits are plotted according to the criteria shown in Eqs. (58) and (69), respectively. The region above the solid (dashed) line is stable for the bunch's rms-emittance (centroid) motion. Note that $\langle y\rangle(0)=0.1$ [cm], $\varepsilon_{\rm rms}(0)=0.01$ [cm], and $\Delta\varepsilon_{\rm rms}$ is rounded to the closest integer.

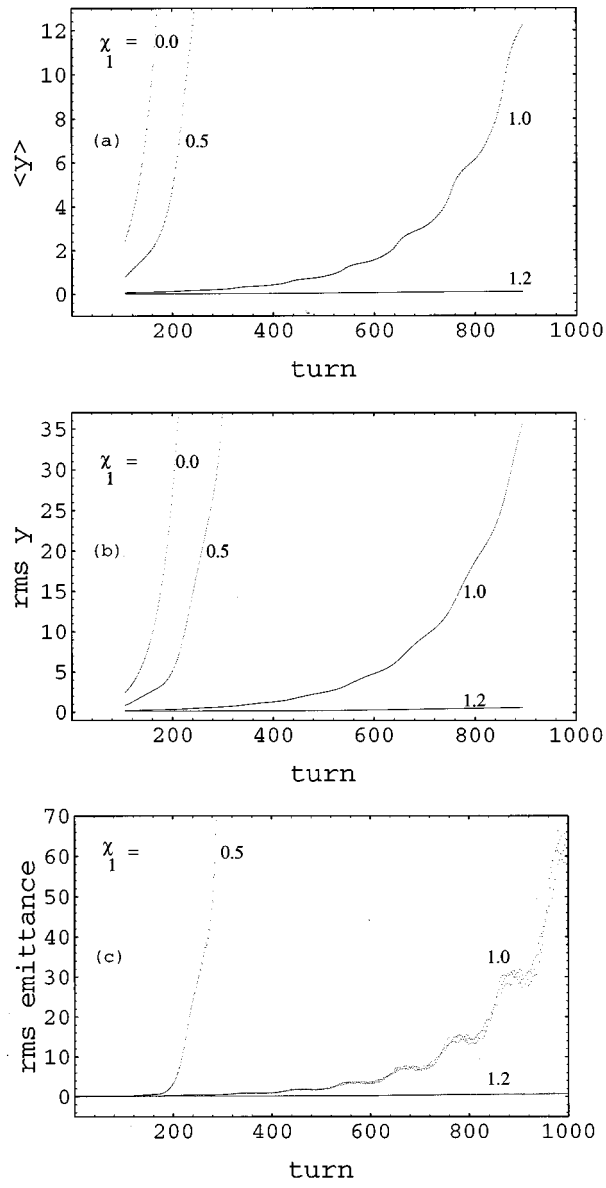

FIG. 16. Multiparticle simulation results showing stabilization of the SHT motions of (a) the centroid, (b) the rms size, and (c) the rms emittance of a Gaussian beam by χ_1, where the SHT stability limit is $\Upsilon<1$ (when $\chi_1=0$). In these figures, $\chi_0=0$ and $\Upsilon=1.65$. See Eqs. (6) and (7) for definitions of χ_0, χ_1, and Υ.

stability criterion. The physics of the underlying mechanism is simple: Landau damping and rotation of the head-tail phase (such that the ac part of the chromaticity does not cause instabilities). Studies of practical operation issues, such as the design of rapidly modulated sextupole magnets; and theoretical issues, such as the reduction of dynamic apertures, as well as exact calculations including the azimuthal mode-coupling, are required. Also, the practical aspects of the varying chromaticity must be compared with the other schemes that also introduce an incoherent tune spread, e.g., space charge, ion trapping, rf nonlinearity, and octopole magnets. Finally, this work suggests that temporal variation of accelerator parameters might be useful in control of other instabilities.

ACKNOWLEDGMENTS

We are grateful to Sasha A. Zholents, who called our attention to the paper by Nakamura. We also thank Alexander W. Chao for his helpful discussion. In particular, W.-H. C. would like to thank Robert L. Gluckstern for his introduction of the concept of alternating phase focusing (APF) which inspired the early idea of this work. This work was supported by the U.S. Department of Energy under Contract Nos. DE-FG-03-95ERA40936 and DE-AC-03-76SF00098.

APPENDIX A: PERIODICITY OF VARYING CHROMATICITY

In this appendix, by using a two-particle model, we show that the periodicity of the chromaticity modulation n must be an odd number, such that the ac part of the chromaticity does not cause additional HT instability. For a two-macroparticle system, the longitudinal motion of the two macroparticles is prescribed as

$$z_{1,2}=\pm\hat{z}\,\sin\,\phi_z,\quad \delta_{1,2}=-\frac{z'_{1,2}}{\eta}=\mp\frac{\omega_s\hat{z}}{c\,\eta}\cos\,\phi_z, \tag{A1}$$

where $\hat{z}$ is the oscillation amplitude with respect to the bunch center, and the upper (lower) sign denotes for the first (second) particle. The transverse motion in the first half-synchrotron period, i.e., $0<s/c<T_s/2$, can be described as follows:

$$y_1''+\frac{\omega_\beta^2(\delta_1)}{c^2}y_1=0, \tag{A2}$$

$$y_2''+\frac{\omega_\beta^2(\delta_2)}{c^2}y_2=-\frac{Nr_0}{2\gamma C}W_\perp y_1, \tag{A3}$$

where a constant short-range transverse wake $W_\perp$ is assumed. For the second half-period, i.e., $T_s/2<s/c<T_s$, $y_1\leftrightarrow y_2$.

According to Eqs. (1), (3), and (A1), the betatron frequencies of the head and tail split as

$$\omega_{\beta 1,2}(s)=\omega_{\beta 0}\mp\omega_s\sum_{n=0}\chi_n\cos\,\phi_z\cos(n\phi_z+\theta_n). \tag{A4}$$

The approximate solution of Eqs. (A3) can be found by assuming

$$y_{1,2}(s)=Y_{1,2}(s)\exp[-i\Phi_{1,2}(s)], \tag{A5}$$

where both $Y(s)$ and $\Phi(s)$ vary slowly compared with the betatron oscillation,

$$\Phi_{1,2}(s)=\int_0^s ds'\,\frac{\omega_{\beta 1,2}(s')}{c}=\omega_{\beta 0}\frac{s}{c}\mp\frac{1}{2}\sum_{n=0}\chi_n g_n, \tag{A6}$$

and

$$g_n(n\neq 1)=\cos\ \theta_n\left[\frac{\sin(n+1)\phi_z}{n+1}+\frac{\sin(n-1)\phi_z}{n-1}\right]+\sin\ \theta_n\left[\frac{\cos(n+1)\phi_z-1}{n+1}+\frac{\cos(n-1)\phi_z-1}{n-1}\right], \tag{A7}$$

$$g_1=\cos\ \theta_1(\tfrac{1}{2}\sin 2\phi_z+\phi_z)+\tfrac{1}{2}\sin\ \theta_1(\cos 2\phi_z-1). \tag{A8}$$

Substituting Eq. (A5) into Eq. (A3) and neglecting the small parts, where

$$(|Y_2''/Y_2|,|\Phi_2''|)\ll|\Phi_2'Y_2'/Y_2|\simeq\omega_{\beta 0}Y_2'/cY_2 \tag{A9}$$

and $\omega_s\ll\omega_{\beta 0}$, leads to

$$Y_2'(s)\simeq i2\frac{\omega_s}{c\pi}\Upsilon Y_1(0)\exp\left(i\sum_{n=0}\chi_n g_n\right). \tag{A10}$$

Integration of Eq. (A10) leads to

$$Y_2(cT_s/2)\simeq Y_2(0)+i2\Upsilon S_I Y_1(0), \tag{A11}$$

where

$$S_I=\frac{1}{\pi}\int_0^{\pi}d\phi_z\ \exp\left(i\sum_{n=0}\chi_n g_n\right). \tag{A12}$$

Similarly, for the second half-synchrotron period, we have

$$Y_1(cT_s)\simeq Y_1(cT_s/2)+i2\Upsilon S_{II}Y_2(cT_s/2), \tag{A13}$$

where

$$S_{II}=\frac{1}{\pi}\int_{\pi}^{2\pi}d\phi_z\ \exp\left(-i\sum_{n=0}\chi_n h_n\right), \tag{A14}$$

and

$$h_n(n\neq 1)=\cos\ \theta_n\left[\frac{\sin(n+1)\phi_z}{n+1}+\frac{\sin(n-1)\phi_z}{n-1}\right]+\sin\ \theta_n\left[\frac{\cos(n+1)\phi_z-(-1)^{n+1}}{n+1}+\frac{\cos(n-1)\phi_z-(-1)^{n-1}}{n-1}\right], \tag{A15}$$

$$h_1=\cos\ \theta_1(\tfrac{1}{2}\sin 2\phi_z+\phi_z-\pi)+\tfrac{1}{2}\sin\ \theta_1(\cos 2\phi_z-1). \tag{A16}$$

The amplitudes of the two-particle system after a complete synchrotron period can therefore be written as

$$\boldsymbol{V}(s/c=T_s)=\boldsymbol{M}_{II}\boldsymbol{M}_I\boldsymbol{V}(s/c=0)=\boldsymbol{M}\boldsymbol{V}(0), \tag{A17}$$

where $\boldsymbol{V}=(Y_1,Y_2)^T$, and the transfer map is

$$\boldsymbol{M}=\begin{bmatrix}1 & i2\Upsilon S_{II}\\ 0 & 1\end{bmatrix}\begin{bmatrix}1 & 0\\ i2\Upsilon S_I & 1\end{bmatrix}=\begin{bmatrix}1-4\Upsilon^2 S_I S_{II} & i2\Upsilon S_{II}\\ i2\Upsilon S_I & 1\end{bmatrix}. \tag{A18}$$

The eigenvalues of $\boldsymbol{M}$ are

$$\lambda=1-2\Upsilon^2 S\pm\sqrt{4\Upsilon^2 S(\Upsilon^2 S-1)}, \tag{A19}$$

where $S=S_IS_{II}$. Note that when the chromaticity is constant, and the head-tail phase is small, i.e., $n=0$ and $\chi_0\ll 1$, we have $S_I=S_{II}\simeq 1+4i\chi_0/\pi$ [9]. When the chromaticity is zero, i.e., $\chi_0=0$, and $\Upsilon<1$, the modulus of the eigenvalue is 1 and the system is stable. The value $\Upsilon=1$ corresponds to the threshold of the SHT instability.

To investigate the stability of the two-particle system, we first discuss the situation when the head-tail phase is small, i.e., $\chi_n\ll 1$. The functions S_I and S_{II} can then be approximated as

$$S_I\approx 1+i\sum_{n=0}\chi_n G_n, \tag{A20}$$

$$S_{II}\approx 1-i\sum_{n=0}\chi_n H_n, \tag{A21}$$

where

$$G_n(n\neq 1)=\int_0^{\pi}d\phi_z g_n(\phi_z)=\frac{1}{\pi}\cos\theta_n\left[\frac{1+(-1)^n}{(n+1)^2}+\frac{1+(-1)^n}{(n-1)^2}\right]-\sin\ \theta_n\left(\frac{1}{n+1}+\frac{1}{n-1}\right), \tag{A22}$$

$$H_n(n\neq 1)=\int_{\pi}^{2\pi}d\phi_z h_n(\phi_z)=-\frac{1}{\pi}\cos\ \theta_n\left[\frac{1+(-1)^n}{(n+1)^2}+\frac{1+(-1)^n}{(n-1)^2}\right]+\sin\ \theta_n\left[\frac{(-1)^n}{n+1}+\frac{(-1)^n}{n-1}\right], \tag{A23}$$

and

$$G_1=H_1=\frac{\pi}{2}\cos\ \theta_1-\tfrac{1}{2}\sin\ \theta_1. \tag{A24}$$

The product of S_I and S_{II} in Eq. (A19) is then

$$S=S_IS_{II}=1+\sum_{n,m=0}\chi_n\chi_m G_nH_m+i\sum_{n=0}\chi_n(G_n-H_n). \tag{A25}$$

Note that, in Eqs. (A20) and (A21), the real part of $S_I(S_{II})$ is the resonant term, and the imaginary part is the chromatic term, in the first (second) half of a synchrotron period. Examining the form of the eigenvalue λ, the stability condition is, in general, when

$$S\in\mathrm{Re},\quad S>0\quad\text{and}\quad\Upsilon^2<1/S, \tag{A26}$$

where the modulus of eigenvalue of the transfer map $\boldsymbol{M}$ equals 1, i.e. $|\lambda|=1$. Since $G_n-H_n=0$, when

$$n \subset odd, \tag{A27}$$

or

$$n \subset even \quad \& \quad \theta_n = \tan^{-1}\left[\frac{2(n^2+1)}{\pi n(n^2-1)}\right], \tag{A28}$$

which makes the imaginary part of S vanish, we conclude that the stability conditions of the head-tail instability with the varying chromaticity when $\chi_n \ll 1$, are Eqs. (A26)–(A28). Note that, in the case when the chromaticity is a constant, i.e. when $n=0$ only, we have $G_0 - H_0 = 8/\pi$, $\mathrm{Im}(S) \neq 0$, and $|\lambda| \neq 1$, the two-particle system is inherently unstable.

In other words, for a small head-tail phase χ_n, using the varying chromaticity with an odd function of synchrotron oscillation period, one can build up a stability threshold for Υ from zero to $1/\sqrt{S}$. An odd function for the chromaticity can be achieved, by either alternating the sign of ξ or modulating ξ by a sinusoidal function within a synchrotron period.

APPENDIX B: MULTIPARTICLE SIMULATION

A simulation code has been developed, which follows the motion of macroparticles that are initially loaded with a bi-Gaussian distribution in both longitudinal and transverse phase spaces. The motion of each particle is determined by Eqs. (4) and (5), which are transformed into a four-dimensional map for particle's transverse and longitudinal motions.

Specifically, the code simulates a bunched beam traversing a ring with a transverse impedance. The momentum P_y is changed by the kick of the transverse wake force, where $P_y = (c/\omega_{\beta 0})y'$. The particle's betatron oscillation is carried out by a rotation matrix, where Eqs. (1) and (2) are used for the angular frequency. In most cases, a uniform transverse wake function is used. No longitudinal wake force is included. Results are numerically converged when the number of macroparticles simulated is larger than 400.

The accelerator parameters used in the simulations are listed in Table II, which can be scaled according to the three parameters: Υ, χ_0, and χ_1. The curve of $\langle y \rangle$ presented in this paper is the bunch centroid motion averaged over a synchrotron period. It is defined as

TABLE II. Parameters used in the simulations.

Particle's classical radius r_0 (cm)	1.534×10^{-16}
Number of particles per bunch N	2×10^{11}
Energy E (GeV)	40
Circumference C (m)	6400
Slippage factor η	10^{-3}
Synchrotron tune ν_s	0.0094
Betatron tune $\nu_{\beta 0}$	16.35
rms bunch length σ_z (cm)	1
Shunt impedance R_s (Ω)	3000
Pipe radius b (cm)	3.0
Chromaticity ξ_0	0.1246
Initial beam transverse offset Δy (cm)	0.1
Initial rms bunch size σ_y (cm)	0.1
Initial rms emittance $\varepsilon_{\mathrm{rms}}$ (cm)	0.01
Head-tail phase χ_0	0.02
Intensity parameter Υ	0.22

$$\langle y \rangle(\tau_n) = \left[\frac{1}{2N_s+1}\sum_{i=\tau_n-N_s}^{\tau_n+N_s} \overline{y^2}(i)\right]^{1/2}, \tag{B1}$$

$$y_{\mathrm{rms}}(\tau_n) = \left[\frac{1}{2N_s+1}\sum_{i=\tau_n-N_s}^{\tau_n+N_s} \sigma_y^2(i)\right]^{1/2}, \tag{B2}$$

where

$$\overline{y(i)} = \frac{1}{N_m}\sum_{m=1}^{N_m} y_m(i), \qquad \sigma_y^2(i) = \frac{1}{N_m}\sum_{m=1}^{N_m}[y_m(i) - \overline{y(i)}]^2, \tag{B3}$$

N_m is the number of macro-particles used in the simulations, τ_n is the number of turn, and N_s is the integer part of $1/\nu_s$. The rms emittance is defined as

$$\varepsilon_{\mathrm{rms}}(\tau_n) = \sqrt{\sigma_y^2(\tau_n)\sigma_{P_y}^2(\tau_n) - \sigma_{y-P_y}^2(\tau_n)}, \tag{B4}$$

where

$$\sigma_{y-P_y}^2(\tau_n) = \frac{1}{N_m}\sum_{m=1}^{N_m}[y_m(\tau_n) - \overline{y(\tau_n)}][P_{ym}(\tau_n) - \overline{P_y}(\tau_n)]. \tag{B5}$$

[1] BNS damping is used for the beam breakup in linear accelerators, in which the transverse wake is compensated by chirping the betatron frequency using RFQ or tilting the energy spread using rf. See V. Balakin, A. Novokhatsky, and V. Smirnov, *Proceedings of the 12th International Conference on High Energy Accelerators, Fermilab* (Fermilab, Batavia, 1983), p. 119.

[2] W.-H. Cheng, A. M. Sessler, and J. S. Wurtele, Phys. Rev. Lett. **78**, 4565 (1997); Lawrence Berkeley National Laboratory Report No. LBNL-39642, 1996 (unpublished).

[3] The SPEAR Group, J. M. Paterson *et al.*, in *Proceedings of the 9th International Conference on High Energy Accelerators, SLAC, 1974* (Stanford University, Stanford, 1974), p. 338; J. Gareyte and F. Sacherer, *ibid.* p. 341; Y. Miyahara and K. Takata, Part. Accel. **10**, 125 (1980).

[4] C. Pellegrini, Nuovo Cimento A **64**, 447 (1969); M. Sands, SLAC Report Nos. TN-69-8 and TN-69-10 (1969) (unpublished); F. Sacherer, *Proceedings of the 9th International Conference on High Energy Accelerators, SLAC, 1974* (Ref. [3]), p. 347.

[5] R. H. Siemann, in *Physics of High Energy Particle Accelera-*

tors, edited by Melvin Month, Peri F. Oahl, and Margaret Dienes, AIP Conf. Proc. No. 127 (AIP, New York, 1984), p. 368; R. H. Siemann, Nucl. Instrum. Methods Phys. Res. Sect. A **221**, 293 (1984).

[6] E. Gianfelice (unpublished); F. Galluccio, Part. Accel. **50**, 141 (1995).

[7] R. Cappi, Part. Accel. **28**, 117 (1995).

[8] E. Kikutani, Part. Accel. **52**, 251 (1996).

[9] A. W. Chao, *Physics of Collective Instabilities in High Energy Accelerators* (Wiley, New York, 1993).

[10] K. Johnsen, *Proceedings of the CERN Symposium on High Energy Accelerators and Pion Physics, Geneva, 1956* (CERN, Geneva, 1956), Vol. 1, p.106; K. Takayama, Part. Accel. **14**, 201 (1984); S. Y. Lee and J. M. Wang, IEEE Trans. Nucl. Sci. **NS-32**, 2323 (1985); J. Wei and S. Y. Lee, Part. Accel. **28**, 77 (1990).

[11] T. Nakamura, in *Proceedings of the 1995 IEEE Particle Accelerator Conference* (IEEE, Dallas, 1995), Vol. 5, p. 3100.

[12] D. Boussard (unpublished).

[13] I. S. Gradshteyn and I. M. Ryzhik, *Table of Integrals, Series, and Products*, 5th ed. (Academic, San Diego, 1994).

[14] A. Hofmann, CERN Report No. 89-01 (1989) (unpublished).

[15] L. D. Landau, J. Phys. U.S.S.R. **10**, 25 (1946); N. G. van Kampen, Physica (Amsterdam) **21**, 949 (1955); F. J. Sacherer (unpublished); Y. Chin, K. Satoh, and K. Yokoya, Part. Accel. **13**, 45 (1983).